PHYSICAL REVIEW A VOLUME 53, NUMBER 2 FEBRUARY 1996

Ab initio potential-energy surfaces and electron-spin-exchange cross sections for H-O_2 interactions

James R. Stallcop and Harry Partridge

Computational Chemistry Branch, Space Technology Division, NASA Ames Research Center, Moffett Field, California 94035-1000

Eugene Levin

Thermosciences Institute, NASA Ames Research Center, Moffett Field, California 94035-1000

(Received 20 April 1995)

Accurate quartet- and doublet-state potential-energy surfaces for the interaction of a hydrogen atom and an oxygen molecule in their ground states have been determined from an *ab initio* calculation using large-basis sets and the internally contracted multireference configuration interaction method. These potential surfaces have been used to calculate the H-O_2 electron-spin-exchange cross section; the square root of the cross section (in a_0), not taking into account inelastic effects, can be obtained approximately from the expressions $2.390E^{-1/6}$ and $5.266-0.708\log_{10}(E)$ at low and high collision energies E (in E_h), respectively. These functional forms, as well as the oscillatory structure of the cross section found at high energies, are expected from the nature of the interaction energy. The mean cross section (the cross section averaged over a Maxwellian velocity distribution) agrees reasonably well with the results of measurements.

PACS number(s): 34.20.Ma, 34.50.−s

I. INTRODUCTION

Spin-exchange collisions are of interest for studies of gases of the upper atmosphere [1] and interstellar space [2]. Accurate interaction energies [3,4] have allowed accurate calculations [5–7] of the spin-flip cross sections for the collision of hydrogen atoms; the theoretical results agree well with measured data [8]. On the other hand, the comparison for H-O_2 is considerably less satisfactory; spin-flip-scattering calculations with accurate interaction energies have been recommended [9,10] to help resolve differences in measured data.

Walch and co-workers [11–13] have reported extensive *ab initio* calculations to define the ground-state HO_2 potential-energy surface; references to earlier work are contained therein. Unfortunately, their results do not include the potential data for large H-O_2 separation distances that are required to determine spin-flip cross sections, especially at lower collision energies. We have calculated accurate H-O_2 potential-energy surfaces for the doublet and quartet states, corresponding to an interaction of the atom and molecule in their ground states, for a broad range of separation distances. We have extended these results with the proper long-range forces to determine transport collision integrals [14(a)] and spin-flip cross sections for a broad range of energies. A description of the molecular-structure calculations and the construction of the potential-energy surfaces is presented along with results in Sec. II. Approximations to the spin-flip cross sections and an outline of the scattering calculation can be found in Sec. III; the spin-flip cross sections from the scattering calculation are presented and compared with approximations and measured data in Sec. IV. Concluding remarks are contained in Sec. V.

II. DETERMINATION OF THE POTENTIAL-ENERGY SURFACES

The potential-energy curves are determined from *ab initio* calculations using the complete-active-space self-consistent-field (CASSCF)–internally contracted multireference configuration interaction (ICMRCI) method [15,16]. The calculations are performed in C_s symmetry with the oxygen $2p$ orbitals and the hydrogen $1s$ orbital active. The oxygen $2s$ orbitals are correlated in the CI calculation, but are constrained to be doubly occupied in all reference configurations. A multireference analog of the Davidson correction [17,18] $(+Q)$ is used to estimate the effect of higher excitations.

The one-particle basis sets employed are the augmented correlation-consistent polarized-valence basis sets by Dunning and co-workers [19,20]. The triple-ζ (TZ) basis set was employed for extensive calculations that could define a complete and nearly complete potential-energy surface for the doublet and quartet states, respectively. A smaller number of calibration calculations were performed employing the larger quadruple-ζ (QZ) basis set. Basis-set superposition errors (BSSE's) were determined using the counterpoise method [21]. The *ab initio* energies corresponding to the QZ calculation will be tabulated elsewhere [14(b)], both the TZ and QZ results are, however, available from the authors.

The coordinate system for the present work is specified by the separation distance r of the H atom from the center of mass of O_2 and an angle γ between a line from H to the center of mass of O_2 and the O_2 symmetry axis passing through the nuclear centers. Making a rigid-rotor approximation for O_2, the O-O separation distance r_{OO} is fixed at the equilibrium value $2.28a_0$. For scattering calculations, a better choice for r_{OO} would be the expectation value for the first vibrational state; however, since the size of the spin-flip cross section is primarily determined by the interaction energies at large r (see the analysis of Sec. III below), one expects that the correction to the spin-flip cross section from this slightly larger value for r_{OO} will not be significant, i.e., within the uncertainty of the present scattering calculation. The potential energy curves $V(r,\gamma)$ derived from the present

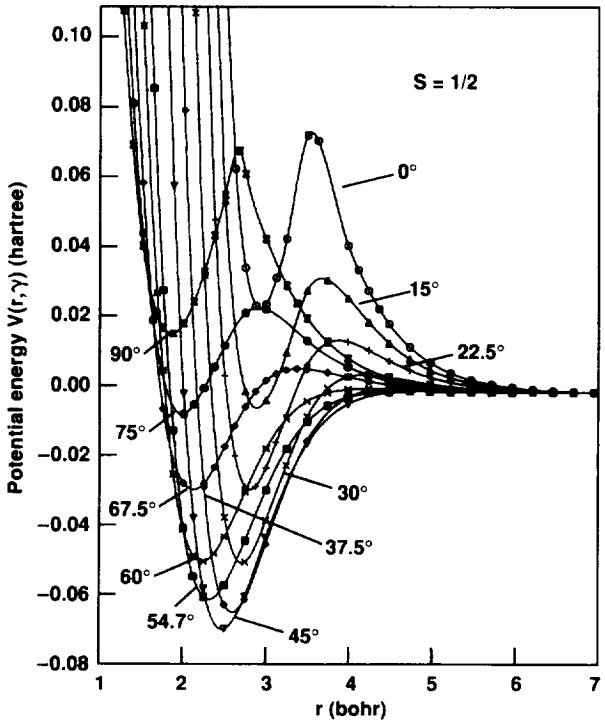

FIG. 1. H-O_2 potential-energy curves for the doublet state for various values of the angle γ. All curves were constructed from spline fits to the discrete data.

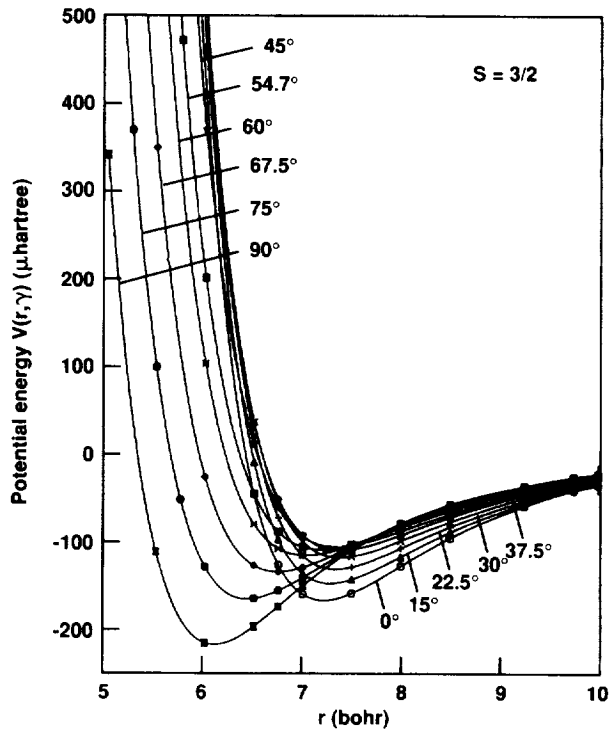

FIG. 2. H-O_2 potential-energy curves for the quartet state for various values of the angle γ. All curves were constructed from spline fits to the discrete data.

calculation are shown in Figs. 1 and 2, for the doublet and quartet states, respectively.

The doublet-state potential-energy curves for six values of γ (0°, 30°, γ_0, 60°, 75°, and 90°) were determined from QZ calculations. The angle $\gamma_0 \approx 54.7°$ is defined by the condition

$$P_2(\cos\gamma_0)=0, \tag{1}$$

where P_2 is a Legendre polynomial of order 2; the potential energy at this angle is of interest for scattering calculations (see Sec. IV below) since it becomes a good approximation to the spherically averaged potential energy at large r. These curves and the results of the TZ calculations were then used to construct curves for additional values of γ. Corrections to the TZ results were obtained from least-squares fits to the energy differences $\Delta V(r,\gamma)$, between the energies from the QZ and TZ calculations, using Legendre polynomials $P_n(\cos\gamma)$ with n restricted to even values by symmetry. For large r, where the correction is relatively large because of BSSE's for the TZ results, we found that the corresponding fit to the logarithm of $\Delta V(r,\cos\gamma)$ yielded higher accuracy for the predicted corrections. Some of the data points at about $3.5a_0$ for the potential-energy barriers, shown in Fig. 1, for small γ had to be determined directly from QZ calculations; here the fitting is not accurate because of the large variation in ΔV as γ approaches zero. In addition, the TZ results were used to construct the potential-energy walls at small r; here the improvement from the QZ calculation is expected to have only a negligible effect on the results of the present scattering calculation. Furthermore, taking into account the rigid-rotor approximation for O_2 of the present calculation, one expects that these QZ calculations will most likely not yield a meaningful change in the scattering results.

The quartet-state potential-energy curves were constructed from the results of the QZ calculation for the same angles used for the doublet case, excluding 60°. The curves for $\gamma=15°$ and 45° were obtained by the fitting procedure for the energy corrections described above for the doublet case. Because of the more uniform behavior of the quartet potential-energy surface (in contrast to the complex nature of the corresponding doublet-state curves arising from avoided curve crossings [11–13]) fewer curves at different values of γ are required to define a complete potential energy surface. The curves for remaining values of γ shown in Fig. 2 were determined from least-squares fits to the potential-energy data for the above seven values of γ, using the P_n and the procedures described in the preceding analysis. As in the doublet case, the repulsive walls for the quartet state were also constructed from the results of the TZ calculation at small r.

The coefficients of the various polynomial fits that are described above, are tabulated in Ref. [14(b)] to facilitate the determination of $V(r,\gamma)$ for values of γ not covered in this work. The accuracy of the potential data from the fitting procedures was determined by comparison with the results of QZ calculations. At large r, for example, we found that for the quartet state the predicted values of $V(r,75°)$ determined from fits to $\ln\Delta V$ using only the data for the other four angles (0°, 30°, γ_0, and 90°) agree with the corresponding energies from the QZ calculation to within 1% in the van der Waals region ($r \geq 5a_0$). Another confirmation of accuracy will be pointed out in the following paragraph.

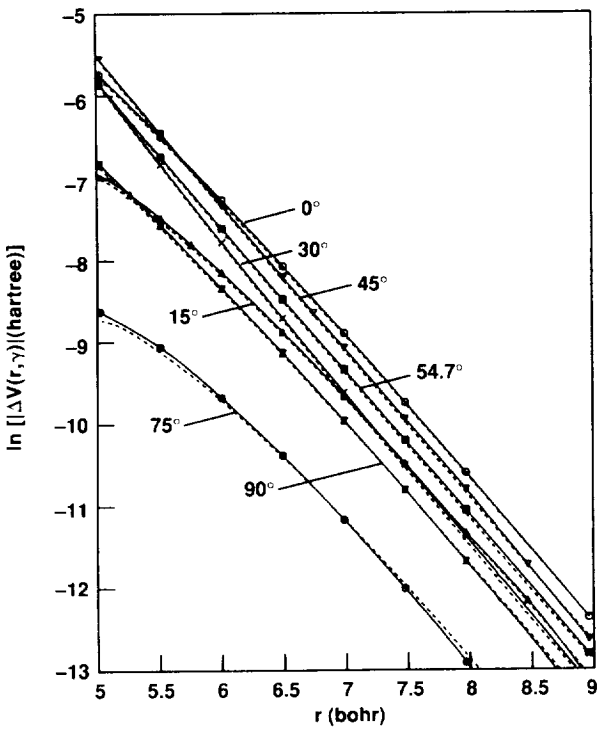

FIG. 3. Energy difference between the potential energies of the quartet and doublet states for selected values of the angle γ. A pair of curves, one that represents the QZ (solid line) and another that represents the TZ (dashed line) calculations, is shown for each value of γ.

At higher energies, the size of the spin-flip cross section is (to a first approximation, see Sec. III below) determined by the magnitude of the difference between the potential energies of the doublet and quartet states at large r. The energy difference obtained from the QZ calculation is compared with the corresponding results for the TZ calculation in Fig. 3. The close agreement of the two sets of curves suggests that the present calculation yields a nearly converged (accurate) value for this quantity and therefore that the present potential curves should yield accurate scattering cross sections. Furthermore, the agreement shown by the curves for 15° and 45° provides additional support for the accuracy of the fitting procedure described above.

The *ab initio* curves have been extended at large r with the long-range expansion

$$V(r,\gamma)\rightarrow\sum_{n=3}\frac{\bar{C}_{2n}}{r^{2n}}[1+\Gamma_{2n}P_2(\cos\gamma)] \tag{2}$$

where $\bar{C}_{2n}$ is the isotropic dispersion coefficient and the parameter Γ_{2n} specifies relative anisotropy. For the leading term, we take the value $19.16E_ha_0^6$ for $\bar{C}_6$ determined by Zeiss and Meath [22] from oscillator strength, photoabsorption, and scattering data and the value 0.211 for Γ_6 obtained by Langhoff, Gordon, and Karplus [23] from optical dispersion absorption and scattering data. Noting that the ratios of the dispersion coefficients for interactions involving hydrogen are about the same (e.g., see Ref. [24]), we can obtain estimates of the two higher-order dispersion coefficients using the values of $\bar{C}_{2n}$ calculated by Meyer (as reported in Ref. [25]) for H-H_2; i.e., $8.813E_ha_0^6$, $162.3E_ha_0^8$, and $3999E_ha_0^{10}$, for $n=3$–5, respectively. Hence, finding that the ratio of $\bar{C}_6$ for H-O_2 compared to H-H_2 is 2.17, we obtain the estimates $352E_ha_0^8$ and $8678E_ha_0^{10}$ for $n=4$ and 5, respectively, for the present work.

Values for the higher-order ($n=6$–8) coefficients were obtained from recursion relations [26,27]

$$\bar{C}_{2n+4}=(\bar{C}_{2n+2}/\bar{C}_{2n})^3\bar{C}_{2n-2}. \tag{3}$$

We found that the long-range interaction energy calculated from the above values of $\bar{C}_{2n}$ and Eq. (2) for γ_0 [where the second term within the square brackets of Eq. (2) vanishes] agrees well with the corresponding results from the QZ calculation for this angle at large r. Furthermore, comparing the long-range interaction energy with the results of the QZ calculation for other angles, we found that including the anisotropic contribution for $n=4$ with the value 1.15 for Γ_8 improved the agreement of the values of $V(r,\gamma)$ from Eq. (2) with the corresponding *ab initio* results.

III. THE SCATTERING CALCULATION

A general formulation of the scattering for collision partners, such as the hydrogen atom and the Σ-state oxygen molecule of this study, has been developed by Launay [28] using formalism for the body-fixed system. We have adopted the sudden approximations of Parker and Pack [29] to calculate the scattering in the body-fixed system; the spin-flip cross sections from this approach should be sufficiently accurate, provided the collision energy E is not too low. Applying both the energy and centrifugal sudden approximations of Ref. [29], we find that the the spin-flip cross section (for homonuclear molecules) can be obtained from

$$\sigma_{SF}(E)=\int_0^{\pi/2}\sigma_{SF}(E,\gamma)\sin\gamma\,d\gamma, \tag{4}$$

where the cross sections $\sigma_{SF}(E,\gamma)$ are determined for an orientation specified by the angle γ that remains fixed during the collision. Thus $\sigma_{SF}(E,\gamma)$ can be calculated from a central-field formulation of the scattering [9], i.e., from

$$\sigma_{SF}(E,\gamma)=\frac{\pi}{k^2}\sum_{l=0}^{\infty}(2l+1)\sin^2[\eta_l^4(E,\gamma)-\eta_l^2(E,\gamma)], \tag{5}$$

where l is the angular momentum quantum number and k is the wave number. The scattering phase shifts $\eta_l^\mu(E,\gamma)$ are calculated from the interaction energies for the quartet and doublet states ($\mu=4$ and 2, respectively) at each fixed value of γ.

At this point, we shall pause to examine the behavior of the spin-flip cross section, inferred from the interaction energies described in the preceding section and the above scattering approximations.

We can obtain a low-energy estimate of σ_{SF} by generalizing the analysis of Rapp and Francis [30] for charge-exchange collisions, which is based on the results of Giomousis and Stevenson [31] for a long-range polarization force. Following their arguments for scattering in an attrac-

tive long-range force field, only the penetrating collisions with impact parameters $b \leq b_o$, the impact parameter for classical orbiting, can contribute to spin exchange. Taking the probability of spin exchange to be 1/2 for these collisions [i.e., the average value of $\sin^2$ in Eq. (5) for σ_{SF}], using the semiclassical relation $b=(l+1/2)/k$, and replacing the summation of Eq. (5) by an integration, we obtain

$$\sigma_{SF} \approx \pi \int_0^{b_o} b \, db = \tfrac{1}{2} \pi b_o^2. \tag{6}$$

For a given value of E, b_o specifies that E is equal to the value of the maximum of the potential-energy barrier exhibited by the effective potential energy $V_e(r,b)$, i.e., b_o satisfies

$$E - V_e(r,b_o) = E - E\frac{b_o^2}{r^2} - V(r) = 0, \tag{7}$$

$$\frac{d}{dr} V_e(r,b_o) = 0. \tag{8}$$

Taking the long-range form

$$V(r) = -\frac{C_\nu}{r^\nu} \tag{9}$$

and combining Eqs. (7) and (8), we obtain

$$b_o^2 = \frac{\nu}{2}\left(\frac{\nu}{2}-1\right)^{(2/\nu)-1} (C_\nu/E)^{2/\nu}. \tag{10}$$

The spin-flip cross section can be readily obtained by combining relations (6) and (10); for the case $\nu=6$, we find

$$\sigma_{SF}(E) \approx \frac{3}{2^{5/3}} \pi (C_6/E)^{1/3}. \tag{11}$$

The nearly linear behavior and common slope of the energy difference curves shown in Fig. 3 for the values of γ corresponding to the leading contributors to the scattering indicates that an analytical approximation can also be constructed for the spin-flip cross section at high energies. Approximations to the cross sections of the form (5) have been developed [32,33] for an energy difference that can be represented by an exponential at large r; their application to the present potential-energy data is illustrated in the following section. For the purposes of the present paper, however, we point out that the major contributions to spin flip comes from orientations where the corresponding cross sections can be represented [33] by a linear expansion in $\ln(E)$; i.e.,

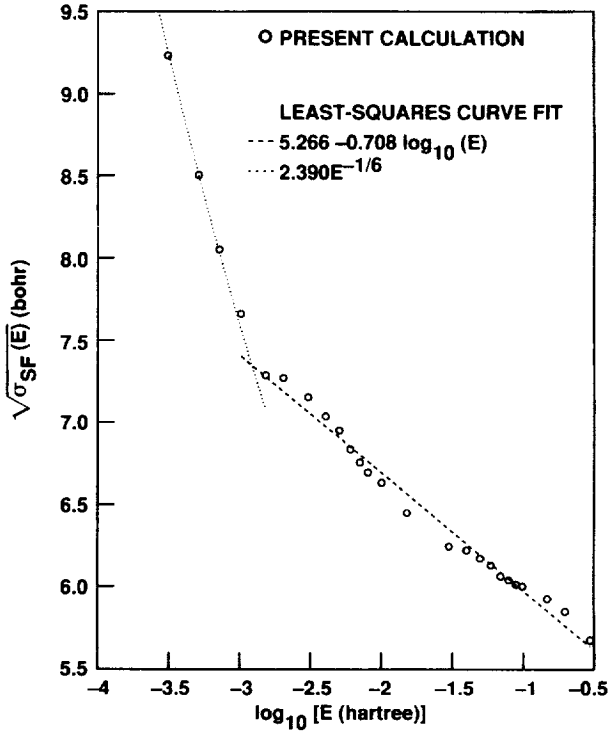

FIG. 4. $H\text{-}O_2$ spin-exchange cross section. The dotted and dashed lines represent the least-squares fits to the discrete data; the fits are based on the functional forms of Eqs. (11) and (12), respectively.

$$[\sigma_{SF}(E,\gamma)]^{1/2} = A(\gamma) + B(\gamma)\ln(E). \tag{12}$$

Provided the variation from the second term on the right-hand side of Eq. (12) is relatively small, it follows from Eq. (4) that $[\sigma_{SF}(E)]^{1/2}$ can also be represented by a linear expansion in $\ln(E)$.

At low energies, the phase shifts for the present work were obtained by direct numerical solution [34] of the Schrödinger equation. At higher energies they were obtained from a semiclassical method that includes a uniform approximation [35,36] that accounts for the quantum-mechanical effects arising from a potential-energy barrier. The integration for Eq. (4) was accomplished with Gaussian quadrature. The results of the scattering calculation are presented and discussed in the following section.

IV. SPIN-FLIP CROSS SECTIONS

The spin-flip cross section from the present calculation is displayed in Fig. 4 along with analytical least-squares fits based on the function forms of the preceding section. The energy dependence of σ_{SF} from Eq. (11) fits the low-energy data well. Taking the value for $\bar{C}_6$ for $H\text{-}O_2$ selected in Sec. II, we find that Eq. (11) yields

$$\sigma_{SF}^{1/2} \approx 2.8 E^{-1/6}, \tag{13}$$

where E is in units of E_h and σ_{SF} is in a_0^2. Comparing this result with the fit shown in Fig. 4, we find that $\sigma_{SF}^{1/2}$ is overestimated by about 17%.

As mentioned above, the potential-energy curve for γ_0 is a good approximation to the spherically averaged potential energy $\bar{V}(r)$ at large r. In previous work [37,38] we have found in some cases that elastic-scattering cross sections determined from $\bar{V}(r)$ can be a good approximation to the corresponding result obtained from the complete potential-energy surface. From a least-squares fit to the present QZ data (see Fig. 3), we obtain

$$V_4(r,\gamma_0)-V_2(r,\gamma_0)=17.31\ \exp(-1.7377r); \quad (14)$$

taking this result (14) and applying the approximate methods [32,33] pointed out in the preceding section, we find

$$[\sigma_{SF}(E)]^{1/2}\approx 5.810-0.882\ \log_{10}(E), \quad (15)$$

where the units are the same as specified for Eq. (13) above. This approximation yields a line that lies slightly below (about 2% lower than) the corresponding calculated data on a semilogarithmic plot such as shown in Fig. 4; i.e., the term corresponding to $A(\gamma)$ of Eq. (12) would require only an increase of about $0.1a_0$ to reach agreement with the results from the scattering calculation. Comparing the values from Eq. (15) with those from the high-energy least-squares fit to the calculated data shown in Fig. 4, we find that $\sigma_{SF}^{1/2}$ for γ_0 is about 12% higher than the mean representing the calculation for the complete potential-energy surface.

Note the oscillatory structure exhibited by the results of the scattering calculation shown in Fig. 4 at higher energies. These oscillations are expected from the behavior of the potential curves shown in Figs. 1 and 2; the presence of potential barriers produces extrema in the difference V_4-V_2. Calculations [36,39] have shown that these extrema cause oscillations in the cross section. In fact, we find such oscillations in $\sigma_{SF}(E,\gamma)$ for those values of γ for which the corresponding potential curves have barriers.

The mean spin-flip cross section, obtained by averaging over a Maxwellian velocity distribution, i.e.,

$$\bar{\sigma}_{SF}(T)=(\kappa T)^{-2}\int_0^\infty \sigma_{SF}(E)E\ \exp(-E/\kappa T)dE, \quad (16)$$

where κ is the Boltzmann constant and T is the kinetic temperature, is of interest for applications. The values of $\sigma_{SF}(T)$ from the results of the present calculation are shown as a function of T in Fig. 5 along with an analytical approximation to facilitate future applications of these results.

We also compare the present results with measured data [40–42] using the corrections of Turner, Snider, and Fleming [10] in Fig. 5. The value from the most recent room-temperature measurements by Anderle *et al.* [42] agrees well with the result from our work. The lowest-temperature measurement of Gordon *et al.* [41] also agrees well with present results; on the other hand, the higher-temperature data fall off more rapidly [more like the $T^{-1/3}$ low-temperature extrapolation expected from $\sigma_{SF}(E)$ with the energy dependence of Eq. (11); see Fig. 5].

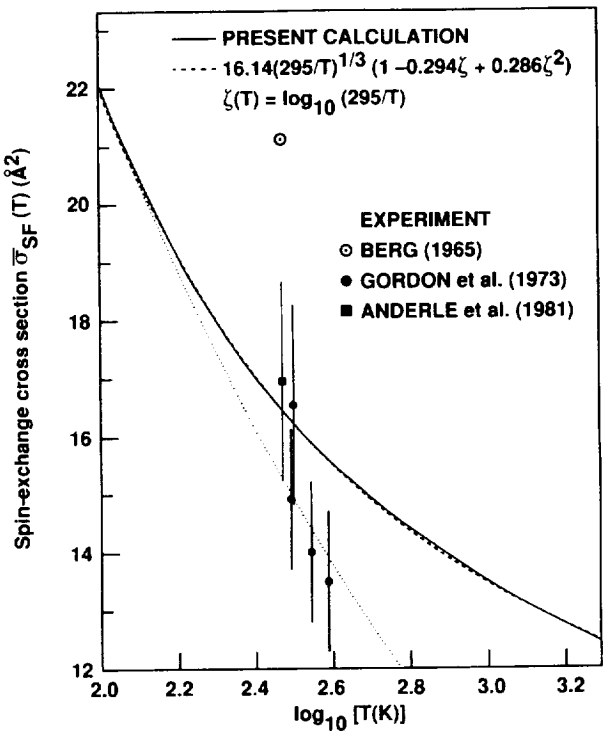

FIG. 5. H-O_2 mean spin-flip cross sections in Å^2 from the results of the present calculation (solid line) and from measured data (the vertical lines represent the error bars for the corresponding data point). The dashed line represents an analytical approximation to the present results. The dotted line was determined from the value (21.85 Å^2) of spin-flip cross section at 100 K from the present results and the temperature dependence of $\sigma_{SF}(T)$ that is obtained from Eq. (16), if $\sigma_{SF}(E)$ is proportional to $E^{-1/3}$ as in Eq. (11).

V. CONCLUDING REMARKS

We have determined the rigid-rotor H-O_2 potential-energy surfaces that cover the complete range of separation distances including the long-range interaction energies required for calculating scattering cross sections. Our analysis indicates that the energy difference between the quartet and the doublet states obtained from our results is very accurate at large separation distances and consequently that the present potential-energy data should allow an accurate determination of the spin-flip cross section. The present scattering results should be accurate at the higher energies, but at lower energies the present potential data merit a more accurate treatment than that of the present calculation. For example, at large impact parameters, one might follow the approach of Stallcop [43] that retains only the energy sudden approximation. Another approach has been mentioned in the beginning of Sec. III above.

We have compared low- and high-energy approximations for σ_{SF} with the scattering results of the present work; this comparison should contribute to the understanding of the physics of collision-induced spin-flip processes and the application of the approximations for estimating $\sigma_{SF}(E)$ from limited potential-energy data.

ACKNOWLEDGMENT

Support for E.L. provided by Contract No. NASA-14031 from NASA to the Eloret Corporation is gratefully acknowledged.

[1] D. R. Bates, Proc. Phys. Soc. London Sect. B **64**, 805 (1951).
[2] G. B. Field, in *The Distribution and Motion of Interstellar Matter in Galaxies*, edited by L. Woltjer (Benjamin, New York, 1962).
[3] W. Kolos and L. Wolniewicz, J. Chem. Phys. **43**, 2429 (1965).
[4] W. Kolos and L. Wolniewicz, Chem. Phys. Lett. **24**, 457 (1974).
[5] A. C. Allison and A. Dalgarno, Astrophys. J. **158**, 423 (1969).
[6] A. C. Allison, Phys. Rev. A **5**, 2695 (1972).
[7] A. J. Berlinsky and B. Shizgal, Can. J. Phys. **58**, 881 (1980).
[8] M. Desaintfucien and C. Audoin, Phys. Rev. A **13**, 2070 (1976).
[9] M. Senba, D. G. Fleming, D. J. Arseneau, D. M. Garner, and I. D. Reid, Phys. Rev. A **39**, 3871 (1989).
[10] R. E. Turner, R. F. Snider, and D. G. Fleming, Phys. Rev. A **41**, 1505 (1990).
[11] S. P. Walch, C. M. Rolfing, C. F. Melius, and C. W. Bauschlicher, J. Chem. Phys. **88**, 6273 (1988).
[12] S. P. Walch and C. M. Rolfing, J. Chem. Phys. **91**, 2373 (1989).
[13] S. P. Walch and R. J. Duchovic, J. Chem. Phys. **94**, 7068 (1991).
[14] (a) H. Partridge, J. R. Stallcop, and E. Levin, in *Molecular Physics and Hypersonic Flows*, edited by M. Capitelli (Kluwer Academic Publishers, Dordrecht, 1966); (b) J. R. Stallcop *et al.* (unpublished).
[15] H.-J. Werner and P. J. Knowles, J. Chem. Phys. **89**, 5803 (1988).
[16] P. J. Knowles and H.-J. Werner, Chem. Phys. Lett. **145**, 514 (1988).
[17] S. R. Langhoff and E. R. Davidson, Int. J. Quantum Chem. **8**, 61 (1974).
[18] M. R. A. Blomberg and P. E. M. Siegbahn, J. Chem. Phys. **78**, 5682 (1983).
[19] T. H. Dunning, J. Chem. Phys. **90**, 1007 (1989).
[20] R. A. Kendall, T. H. Dunning, and R. J. Harrison, J. Chem. Phys. **96**, 6796 (1992).
[21] S. F. Boys and F. Bernardi, Mol. Phys. **19**, 553 (1970).
[22] G. D. Zeiss and W. J. Meath, Mol. Phys. **33**, 1155 (1977).
[23] P. W. Langhoff, R. G. Gordon, and M. Karplus, J. Chem. Phys. **55**, 2126 (1971).
[24] J. R. Stallcop, C. W. Bauschlicher, H. Partridge, S. R. Langhoff, and E. Levin, J. Chem. Phys. **97**, 5578 (1992).
[25] K. T. Tang and J. P. Toennies, Chem. Phys. Lett. **151**, 301 (1988).
[26] K. T. Tang and J. P. Toennies, J. Chem. Phys. **68**, 5501 (1978).
[27] A. J. Thakkar, J. Chem. Phys. **89**, 2092 (1988).
[28] J. M. Launay, J. Phys. B **10**, 3665 (1977).
[29] G. A. Parker and R. T. Pack, J. Chem. Phys. **68**, 1585 (1978).
[30] D. R. Rapp and W. E. Francis, J. Chem. Phys. **37**, 2631 (1962).
[31] G. Giomousis and D. P. Stevenson, J. Chem. Phys. **29**, 294 (1958).
[32] A. Dalgarno, Philos. Trans. R. Soc. London Ser. A **250**, 426 (1958).
[33] J. R. Stallcop and H. Partridge, Phys. Rev. **32**, 639 (1985).
[34] E. Levin, D. W. Schwenke, J. R. Stallcop, and H. Partridge, Chem. Phys. Lett. **227**, 669 (1994).
[35] J. R. Stallcop, NASA Report No. SP-3052, 1969 (unpublished).
[36] J. R. Stallcop, H. Partridge, and E. Levin, J. Chem. Phys. **95**, 6429 (1991).
[37] J. R. Stallcop, H. Partridge, S. P. Walch, and E. Levin, J. Chem. Phys. **97**, 3431 (1992).
[38] H. P. Partridge, C. W. Bauschlicher, J. R. Stallcop, and E. Levin, J. Chem. Phys. **99**, 5951 (1992).
[39] F. J. Smith, Phys. Lett. **20**, 271 (1966).
[40] H. C. Berg, Phys. Rev. **137**, A1621 (1965).
[41] E. B. Gordon, B. I. Ivanov, A. P. Perminov, A. N. Ponomarev, V. L. Tal'roze, and S. G. Khidirov, Pis'ma Zh. Eksp. Teor. Fiz. **17**, 548 (1973) [JETP Lett. **17**, 395 (1973)].
[42] M. Anderle, D. Bassi, S. Iannotta, S. Marchetti, and G. Scholes, Phys. Rev. A **23**, 34 (1981).
[43] J. R. Stallcop, J. Chem. Phys. **61**, 5085 (1974).